CERN-ACC-2015-0213

EuCARD-2

Enhanced European Coordination for Accelerator Research & Development

Journal Publication

Phase field modelling of dynamic thermal fracture in the context of irradiation damage

Schlüter, Alexander (Technische Universität Kaiserslautern) *et al*

01 June 2015

The EuCARD-2 Enhanced European Coordination for Accelerator Research & Development project is co-funded by the partners and the European Commission under Capacities 7th Framework Programme, Grant Agreement 312453.

This work is part of EuCARD-2 Work Package **11: Collimator Materials for fast High Density Energy Deposition (COMA-HDED)**.

The electronic version of this EuCARD-2 Publication is available via the EuCARD-2 web site <http://eucard2.web.cern.ch/> or on the CERN Document Server at the following URL: <http://cds.cern.ch/search?p=CERN-ACC-2015-0213>

Noname manuscript No.
(will be inserted by the editor)

Phase Field Modelling of Dynamic Thermal Fracture in the Context of Irradiation Damage

Alexander Schlüter · Charlotte Kuhn · Ralf Müller · Marilena Tomut · Christina Trautmann · Helmut Weick · Carolin Plate

Received: date / Accepted: date

Abstract This work presents a continuum mechanics approach to model fracturing processes in brittle materials that are subjected to rapidly applied high-temperature gradients. Such a type of loading typically occurs when a solid is exposed to an intense high-energy particle beam that deposits a large amount of energy into a small sample volume. Given the rapid energy deposition leading to a fast temperature increase, dynamic effects have to be considered. Our existing phase field model for dynamic fracture is thus extended in a way that allows modelling of thermally induced fracture. A finite element scheme is employed to solve the governing partial differential equations numerically. Finally, the functionality of our model is illustrated by two examples.

Keywords Phase field · Thermal fracture · Irradiation damage

1 Introduction

The phase field method has become a versatile tool in continuum mechanics. It allows to describe various processes in heterogeneous continua, that range from solidification [2] and phase transformation in a solid [15] to the modelling of ferroelectric materials [16]. The idea of phase field models is to distinguish the different components of a continuum, by means of additional field variables. These phase field variables can be coupled to an underlying physical model. One advantage of phase field models is the implicit description of the evolution of internal surfaces that seperate different phases. For that reason, internal surfaces do not need to be tracked by a special algorithm if numerical methods are used to solve a given problem.

When modelling fracture, the phase field indicates where material is broken and where it is undamaged. Recently proposed phase field models for fracture like in Borden et al. [3], Miehe and Hofacker [8,9] and Kuhn and Müller [12] are based on the variational formulation of brittle fracture by Francfort and Marigo [6], which stems from the energy-based Griffith criterion of fracture mechanics, see Griffith [7]. It has been shown in mathematically oriented works that these phase field models are closely related to the variational model of fracture, see e.g. Chambolle [5]. The publications by Miehe and Hofacker [9], Borden et al. [3] and Schlüter et al. [14] also

A. Schlüter
University of Kaiserslautern
Mailbox 3049
D-67653 Kaiserslautern Tel.: +49 (0) 631 205 3099
Fax: +49 (0) 631 205 2128
E-mail: aschluet@rhrk.uni-kl.de

consider dynamic effects and demonstrate that the phase field approach can capture realistic features of dynamic fracturing. In this work, the model from Schlüter et al. [14] is extended to thermoelasticity. To this end, a similar formulation as proposed in Kuhn and Müller [11] is utilized. The focus is on modelling thermoelastic fracturing due to relativistic particle beams, e.g. heavy ion beams, that hit a solid. Such beams deposit almost instantaneously a huge amount of energy (> 1 GeV) into the solid. Induced energy densities as high as 12 kJ/g result in a rapid temperature rise in a spatially limited region of the solid. Thermoelastic effects finally lead to an expansion of the material inducing elastic waves which can cause complex fracture patterns. For new high-power accelerator facilities such as for instance the future facility for antiprotons and ion research (FAIR)[1] at Darmstadt and other existing or planned neutrino factories, it is of utmost interest to develop reliable models that can predict dynamic fracture under respective loading conditions. Computer-aided calculations are of particular interest for identifying critical operating conditions for the components and for optimized engineering of devices to be exposed to intense particle beams. The numerical method we propose is designed to predict brittle fracture due to irradiation in solid targets. Hence, it is not capable of modelling other causes of failure like phase changes or plastic deformation. It should therefore be considered as a tool to predict fracture in basically two situations:

- The particle beam is of relatively low intensity and the final temperature is significantly lower than the melting or sublimation temperature of the target material. Thus, the whole body can be assumed as linear elastic with constant material parameters.
- The particle beam is of high intensity but causes inelastic behaviour (plastic deformation, phase changes, etc.) only in a confined region of the target. Hence, elastic waves, caused by the beam, propagate in unheated material that can be assumed to be linear elastic with constant material parameters.

In the latter case the results in the vicinity of the beam-spot are not reliable but the model can be used to predict brittle fracture in the remaining parts of the target.

The second section of this work introduces the phase field model and the extension to thermoelasticity whereas section three discusses the numerical method that is used to solve the governing equations. In the fourth section two numerical examples are studied that show the functionality of the model.

2 Phase Field Model

To start with, the phase field model for thermoelastic fracture is presented. The concern of this paper is fracture in brittle materials. Hence, the whole body $\Omega \subset \mathbb{R}^3$ with external boundary $\partial\Omega$ is regarded to be made of linear elastic material with Young's modulus E and Poisson ratio ν, see Fig. 1a). The assumption of linear elastic material behaviour with constant, temperature-independent material properties limits the applicability of the model to temperatures that are well below the melting and sublimation temperature of the irradiated material.

The mechanical behaviour of the body is described in terms of the macroscopic displacement $\boldsymbol{u}(\boldsymbol{x},t)$, linearized strain $\boldsymbol{\varepsilon}(\boldsymbol{x},t)$ and stress $\boldsymbol{\sigma}(\boldsymbol{x},t)$ fields. The mechanical fields have to satisfy DIRICHLET boundary conditions

$$\boldsymbol{u}(\boldsymbol{x},t) \;=\; \boldsymbol{u}^*(\boldsymbol{x},t) \tag{1}$$

on $\partial\Omega_u$ and Neumann boundary conditions

$$\boldsymbol{\sigma}\boldsymbol{n} \;=\; \boldsymbol{t}^* \tag{2}$$

[1] https://www.gsi.de/en/research/fair.htm

on $\partial\Omega_t$, where $\boldsymbol{n}$ is the outward directed normal vector on the boundary $\partial\Omega = \partial\Omega_u \cup \partial\Omega_t$. Additionally, initial conditions for the displacements

$$\boldsymbol{u}\left(\boldsymbol{x}, t_0\right) = \boldsymbol{u}_0\left(\boldsymbol{x}\right) \tag{3}$$

and the velocities

$$\dot{\boldsymbol{u}}\left(\boldsymbol{x}, t_0\right) = \boldsymbol{v}_0\left(\boldsymbol{x}\right). \tag{4}$$

are required. Brittle materials can only sustain small strains. Thus, the linearized strain tensor

$$\boldsymbol{\varepsilon} = \frac{1}{2}\left(\nabla\boldsymbol{u} + \nabla^T\boldsymbol{u}\right) \tag{5}$$

is an appropriate strain measure. The temperature is described by the field $\theta\left(\boldsymbol{x}, t\right)$ which has to satisfy Dirichlet boundary conditions

$$\theta\left(\boldsymbol{x}, t\right) = \theta^*\left(\boldsymbol{x}, t\right) \tag{6}$$

on $\partial\Omega_\theta$ and Neumann boundary conditions that prescribe a heat flux q^* on the boundary $\partial\Omega_q$

$$\boldsymbol{q}\cdot\boldsymbol{n} = q^*. \tag{7}$$

A starting temperature can be included by defining initial conditions

$$\theta\left(\boldsymbol{x}, t_0\right) = \theta_0\left(\boldsymbol{x}\right). \tag{8}$$

Cracks, i.e. internal discontinuities with respect to the macroscopic fields, are denoted as Γ. In order to approximate these discontinuities in a smooth way, a phase field $s(\boldsymbol{x}, t) \in [0, 1]$ is introduced which varies continuously from $s = 1$ in undamaged material to $s = 0$ in fully broken material. This diffusive representation of a crack is also shown in Fig. 1b). Initial conditions for the phase field

$$s(\boldsymbol{x}, t_0) \;=\; 0 \tag{9}$$

can be specified to model existing cracks in the material. The phase field is used to approximate

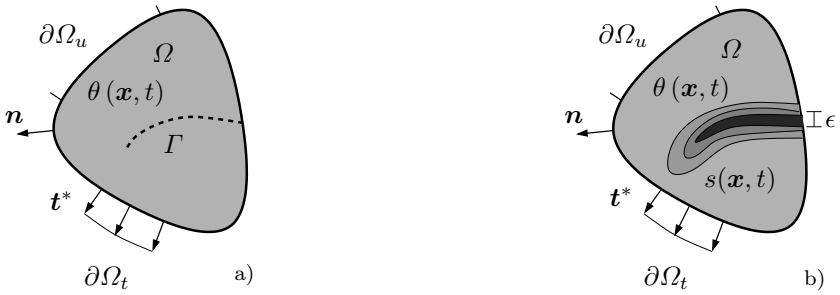

Fig. 1 Body with internal discontinuities (sharp cracks) Γ a), and approximation of internal discontinuities by a phase field $s(\boldsymbol{x}, t)$ b).

the fracture energy that is associated with cracks

$$\int_\Gamma \mathcal{G}_c \,\mathrm{d}A \approx \int_\Omega \mathcal{G}_c \left[\frac{(1-s)^2}{4\epsilon} + \epsilon|\nabla s|^2\right] \mathrm{d}V = E^s. \tag{10}$$

Herein, we assume the fracture resistance $\mathcal{G}_c$ to be a constant that is independent of the temperature, crack speed, radiation history etc. The internal length ϵ controls the width of the phase field approximated crack, see Fig. 1 b). The larger ϵ is, the larger the width of the phase field approximated crack will be. In the limit $\epsilon \to 0$ approximation (10) is exact, see BOURDIN [4]. The total strain (5) can be decomposed in a mechanical part $\boldsymbol{\varepsilon}^e$ and a thermal part $\boldsymbol{\varepsilon}^\theta$, i.e.

$$\boldsymbol{\varepsilon} = \boldsymbol{\varepsilon}^e + \boldsymbol{\varepsilon}^\theta. \tag{11}$$

The mechanical part is a function of the mechanical load $\boldsymbol{\varepsilon}^e = f(\boldsymbol{\sigma})$ and the thermal part can be described by

$$\boldsymbol{\varepsilon}^\theta = \alpha_T (\theta - \theta_0) \mathbf{1}, \tag{12}$$

where $\alpha_T > 0$ is the coefficient of thermal expansion and $\mathbf{1}$ is the identity tensor. Relation (12) is true for materials that expand isotropically when the temperature is increased. If isotropic expansion is not possible due to mechanical restraints on $\boldsymbol{\varepsilon}$, a respective stress state $\boldsymbol{\sigma}$ will result. The phase field s is coupled to the elastic energy that is stored in the body

$$E^e = \int_\Omega \psi_\mathrm{e}(\boldsymbol{\varepsilon}^e, s) \, \mathrm{d}V \tag{13}$$

in order to model the loss of stiffness in broken material. Herein, ψ_e is the elastic energy density which is adopted from Amor et al. [1]

$$\begin{aligned} \psi_\mathrm{e} = {} & \frac{K}{2} \langle \mathrm{tr}(\boldsymbol{\varepsilon}^e) \rangle_-{}^2 \\ & + g(s) \underbrace{\left[\frac{K}{2} \langle \mathrm{tr}(\boldsymbol{\varepsilon}^e) \rangle_+{}^2 + \mu (\boldsymbol{e}^e : \boldsymbol{e}^e) \right]}_{\psi_\mathrm{e}^+} \end{aligned} \tag{14}$$

where

$$\langle \mathrm{tr}(\boldsymbol{\varepsilon}^e) \rangle_- = \begin{cases} \mathrm{tr}(\boldsymbol{\varepsilon})^e & \text{if } \mathrm{tr}(\boldsymbol{\varepsilon}^e) < 0 \\ 0 & \text{else} \end{cases} \tag{15}$$

and

$$\langle \mathrm{tr}(\boldsymbol{\varepsilon}^e) \rangle_+ = \begin{cases} \mathrm{tr}(\boldsymbol{\varepsilon}^e) & \text{if } \mathrm{tr}(\boldsymbol{\varepsilon}^e) \geq 0 \\ 0 & \text{else} \end{cases} . \tag{16}$$

The parameter

$$K = \frac{E}{3(1-2\nu)} \tag{17}$$

is the bulk modulus,

$$\mu = \frac{E}{2(1+\nu)} \tag{18}$$

is the shear modulus and

$$\boldsymbol{e}^e = \boldsymbol{\varepsilon}^e - \frac{\mathrm{tr}(\boldsymbol{\varepsilon}^e)}{3} \mathbf{1} \tag{19}$$

denotes the deviatoric part of the elastic strain tensor. The function $g(s)$ is a degradation function that has to fulfil $g(1) = 1$ and $g(0) = 0$ to model the loss of stiffness in broken material. The property $g'(0) = 0$ is important to make sure that $s \to 0$ if $\psi_\mathrm{e}^+ \to \infty$, see Hofacker and Miehe [9].

In this work we choose $g(s) = s^2$. The expression (14) is intended to allow crack growth only in tensile and shear load states and it also models crack closure via the constitutive law

$$\begin{aligned}\boldsymbol{\sigma} = \frac{\partial \psi_e}{\partial \boldsymbol{\varepsilon}} &= K\langle \mathrm{tr}\,(\boldsymbol{\varepsilon}^e)\rangle_- \mathbf{1} \\ &\quad + g(s)\left[K\langle \mathrm{tr}\,(\boldsymbol{\varepsilon}^e)\rangle_+ \mathbf{1} + 2\mu \boldsymbol{e}^e\right].\end{aligned} \tag{20}$$

Note that the degradation function only affects the positive volumetric and the deviatoric part of $\boldsymbol{\sigma}$. The practicability of the approach is shown by means of a numerical example in Schlüter et al. [14]. An alternative approach based on the spectral decomposition of $\boldsymbol{\varepsilon}$ is presented in Hofacker and Miehe [9]. The kinetic energy is

$$K(\dot{\boldsymbol{u}}) = \int_\Omega \frac{1}{2}\rho \dot{\boldsymbol{u}} \cdot \dot{\boldsymbol{u}}\ \mathrm{d}V. \tag{21}$$

and the work of external forces acting on the boundary $\partial\Omega$ reads

$$P = \int_{\partial\Omega_t} \boldsymbol{t}^* \cdot \boldsymbol{u}\ \mathrm{d}A \tag{22}$$

when body forces are neglected. The fields $\boldsymbol{u}$ and s follow from Hamiliton's principle

$$\delta \int_{t_1}^{t_2} L\ \mathrm{d}t = 0, \tag{23}$$

for arbitrary times $t_1 < t_2$, where L is the Lagrangian

$$L = K - (E^e + E^s - P). \tag{24}$$

The Euler-Lagrange equations of the variational principle (23) are the equation of motion

$$\rho \ddot{\boldsymbol{u}} - \mathrm{div}\boldsymbol{\sigma} = \mathbf{0}, \tag{25}$$

and a phase field equation

$$g'(s)\psi_\mathrm{e}^+ - \mathcal{G}_c \left[2\epsilon \Delta s + \frac{1-s}{2\epsilon}\right] = 0. \tag{26}$$

The evolution of the crack field s, i.e. crack growth, is described by equation (26). Herein, the tensile and shear elastic energy density ψ_e^+ drives crack propagation. The variational principle also yields the Neumann boundary conditions for the displacement, see Eq. (2), and the phase field variable

$$\nabla s \cdot \boldsymbol{n} = 0 \quad \text{on } \partial\Omega. \tag{27}$$

The coupled equations (25) and (26) do not prevent the phase field from recovering, i.e. cracks can heal if the load is removed. Therefore, it is necessary to introduce an additional irreversibility constraint. In this work, irreversibility is modelled by prescribing Dirichlet boundary conditions

$$s(\boldsymbol{x}, t > t^*_{\boldsymbol{x}}) = 0 \quad \text{if} \quad s(\boldsymbol{x}, t^*_{\boldsymbol{x}}) = 0 \tag{28}$$

for the crack field. Herein, $t^*_{\boldsymbol{x}}$ is the time when the crack field becomes zero at the location $\boldsymbol{x}$ for the first time. Another possibility is to enforce that the crack field can only decay, i.e. $\dot{s} < 0$, like it is proposed in Hofacker and Miehe [9].

In addition to brittle fracture which is described by the equation of motion (25) and the phase field equation (26), heat conduction is also included in the model. We choose an isotropic Fourier law as a constitutive relation between the heat flux $\boldsymbol{q}$ and the temperature field

$$\boldsymbol{q} = -\kappa \left(\zeta \left(s^2 + \eta_\theta - 1 \right) + 1 \right) \nabla \theta. \tag{29}$$

This formulation is adopted from Kuhn and Müller [11]. The parameter $\zeta \in [0, 1]$ in Fourier's law defines how the thermal conductivity κ is influenced by a crack. If $\zeta = 0$, the heat flux is not affected by a crack, i.e. the crack is conducting. If $\zeta = 1$ the thermal conductivity is multiplied by $s^2 + \eta_\theta$. Thus, there is no heat flux at cracks, i.e. cracks are isolating. The parameter $\eta_\theta \ll 1$ is a small residual conductivity that is introduced to avoid numerical problems. The field equation for the temperature θ is the energy balance

$$\rho c_p \dot{\theta} = -\nabla \cdot \boldsymbol{q} \tag{30}$$

where the thermoelastic coupling term is neglected. The parameter c_p is the specific heat capacity of the material.

The thermoelastic phase field fracture problem is defined by the field equations

$$\begin{aligned} \rho \ddot{\boldsymbol{u}} - \mathrm{div} \boldsymbol{\sigma} &= \boldsymbol{0}, \\ g'(s) \psi_{\mathrm{e}}^{+} - \mathcal{G}_c \left[2\epsilon \Delta s + \frac{1 - s}{2\epsilon} \right] &= 0, \\ \rho c_p \dot{\theta} &= -\nabla \cdot \boldsymbol{q}, \end{aligned} \tag{31}$$

the constitutive laws

$$\begin{aligned} \boldsymbol{\sigma} &= K \langle \mathrm{tr} \left(\boldsymbol{\varepsilon}^e \right) \rangle_{-} \boldsymbol{1} + g(s) \left[K \langle \mathrm{tr} \left(\boldsymbol{\varepsilon}^e \right) \rangle_{+} \boldsymbol{1} + 2\mu \boldsymbol{e}^e \right], \\ \boldsymbol{q} &= -\kappa \left(\zeta \left(s^2 + \eta_\theta - 1 \right) + 1 \right) \nabla \theta \end{aligned} \tag{32}$$

and the respective boundary and initial conditions.

3 Numerical Method

The numerical approach that is used to solve the coupled set of partial differential equations is only outlined in this section. For a detailed description of the numerical method the reader is referred to Schlüter et al. [14]. The initial boundary value problem is spatially discretized with bilinear isoparametric finite elements, which results in a coupled system of ordinary differential equations of the type

$$\underline{\boldsymbol{R}} \left(\underline{\boldsymbol{d}}, \dot{\underline{\boldsymbol{d}}}, \ddot{\underline{\boldsymbol{d}}} \right) = \underline{\boldsymbol{M}} \ddot{\underline{\boldsymbol{d}}} + \underline{\boldsymbol{D}} \dot{\underline{\boldsymbol{d}}} + \underline{\boldsymbol{P}} \left(\underline{\boldsymbol{d}} \right) - \underline{\boldsymbol{F}} = \underline{\boldsymbol{0}}, \tag{33}$$

where the array of unknowns holds all nodal variables

$$\underline{\boldsymbol{d}} = \left[\boldsymbol{u}_1^T, s_1, \theta_1, \boldsymbol{u}_2^T, s_2, \theta_2, ..., \boldsymbol{u}_N^T, s_N, \theta_N \right]^T \tag{34}$$

of all nodes $I = 1...N$. The matrices $\underline{\boldsymbol{M}}$ and $\underline{\boldsymbol{D}}$ are the global mass and damping matrices respectively, whereas the quantities $\underline{\boldsymbol{P}} \left(\underline{\boldsymbol{d}} \right)$ and $\underline{\boldsymbol{F}}$ describe contributions of internal and external "forces" to the global residual $\underline{\boldsymbol{R}}$. By means of the Newmark method the first and second derivatives with respect to time are approximated at discrete time steps $t_{n+1} = t_n + \Delta t$

$$\begin{aligned} \dot{\underline{\boldsymbol{d}}}_{n+1} &= \dot{\underline{\boldsymbol{d}}}_n + \Delta t \, \ddot{\underline{\boldsymbol{d}}}_\gamma, \text{ where} \\ \ddot{\underline{\boldsymbol{d}}}_\gamma &= (1 - \gamma) \, \ddot{\underline{\boldsymbol{d}}}_n + \gamma \, \ddot{\underline{\boldsymbol{d}}}_{n+1}, \end{aligned} \tag{35}$$

and

$$\begin{aligned} \underline{\boldsymbol{d}}_{n+1} &= \underline{\boldsymbol{d}}_n + \Delta t\ \dot{\underline{\boldsymbol{d}}}_n + \frac{1}{2}\Delta t^2\ \ddot{\underline{\boldsymbol{d}}}_\beta, \text{ where} \\ \ddot{\underline{\boldsymbol{d}}}_\beta &= (1-2\beta)\ \ddot{\underline{\boldsymbol{d}}}_n + 2\beta\ \ddot{\underline{\boldsymbol{d}}}_{n+1} \end{aligned} \tag{36}$$

The parameters are set to $\gamma = 0.5$ and $\beta = 0.5$. With (35) and (36) the global equation (33) yields a nonlinear system of algebraic equations for the nodal unknowns at time t_{n+1}

$$\underline{\boldsymbol{R}}\left(\underline{\boldsymbol{d}}_{n+1}\right) = \underline{\boldsymbol{0}} \tag{37}$$

which is solved with Newton's method. In contrast to the original formulation without thermoelastic coupling, the present model leads to an unsymmetric overall tangent matrix. This has to be considered when choosing an appropriate equation solver.

As proposed in KUHN [10], the irreversibility of the crack growth is modelled by defining homogeneous DIRICHLET boundary conditions for the phase field $s(\boldsymbol{x}, t)$ once the value $s = 0$ is reached for the first time i.e.

$$s_{I,n+1} = 0 \quad \text{if} \quad s_{I,n} = 0. \tag{38}$$

This is accomplished by a reformulation of the residual and the tangent matrix on element level rather than changing global boundary conditions.

4 Simulation of Thermal Fracture

If a solid is exposed to an intense beam of energetic heavy ions, a large amount of energy is absorbed by the material within a short time span. The temperature increases rapidly and strains and stresses are induced in the body due to thermo-elastic expansion which is constrained by the surrounding material. Under these loading conditions, dynamic effects due to elastic waves in the material are expected to be decisive for failure processes. Compared to the speed of elastic waves, thermoelastic effects due to heat conduction are much slower for the considered materials and heat conduction is negligible regarding the short time intervals that will be considered. Thus, the heat equation (30) is not solved but the temperature is prescribed as an external stationary field of defined spatial distribution. The heat conductivity and the specific heat capacity are set to zero, i.e. $\kappa = 0$ and $c_p = 0$.

An axisymmetric finite element formulation of the phase field model from section 3 is employed in the simulations. This means all fields $\boldsymbol{u}, s$ and θ are considered to be independent of the angular coordinate ϕ in a cylindrical r, ϕ, z-coordinate system, see Fig. 2. For this reason not only the geometry but also the loading and boundary conditions are not allowed to break the axial symmetry. These assumptions reduce the computational effort significantly. However, the formation of cracks in radial direction cannot be captured by this reduced model and needs to be addressed in future 3D simulations.

4.1 Cylinder

A cylindrical body is considered that is subjected to a particle beam, see Fig. 2. Since the problem is axisymmetric, it is sufficient to reduce the model to the shaded rectangular area that is also shown in Fig. 2. The temperature load θ^* is assumed to be independent of the z- and ϕ-coordinate and can be expressed as

$$\theta^*(r, t) = \theta_{\max} R(r) T(t), \tag{39}$$

where $R(r)$ is a function of the radial coordinate and $T(t)$ is a function of the time. A temperature field θ^* that is nearly independent of the penetration depth of the particles is a reasonable assumption if the target-beam configuration is set up in such a way that the peak energy deposition, the so-called Bragg peak, lies outside the target geometry, see e.g. Tahir et al. [17]. The highest increase of temperature is expected in the center of the beam, i.e. at $r = 0$mm, whereas the outer parts of the cylinder will not be hit directly. Hence an exponential distribution

$$R(r) = \exp\left(-\left(\frac{r}{r_0}\right)^2\right) \tag{40}$$

is chosen. The length parameter is $r_0 = 0.86$mm. The temperature increases rapidly when the beam hits the body. This is described by the function

$$T(t) = \begin{cases} 0.0 & \text{if } t < t_1 \\ \sin^2\left(\frac{\pi}{2}\frac{t-t_1}{t_e}\right) & \text{if } t_1 \le t \le t_1 + t_e \\ 1.0 & \text{if } t \ge t_1 + t_e \end{cases} \tag{41}$$

which is illustrated in Fig. 4. The loading time scale is $t_e = 10^{-6}$ s and $t_1 = 0$ s. The mesh consists of 165×300 square finite elements. Since the element size is the same for the whole mesh, the computed crack pattern will not be influenced by any mesh-inhomogeneities. The boundaries of the body are all stress free and the phase field is set to $s_0 = 1$ at all nodes, so the material is originally undamaged. The chosen material and model parameters are listed in table 1. These are fictional material properties. Thus, the numerical examples should be considered as an attempt to understand the qualitative features of brittle fracture caused by irradiation. However, realistic material properties, e.g. of isotropic grade high-density graphite, could be used as well but would not result in fracture for the given temperature load. The characteristic length ϵ is connected to the stress at which a phase field crack will nucleate. For the one dimensional case it can be shown that this critical stress is

$$\sigma_c = \frac{3}{16}\sqrt{\frac{3E\mathcal{G}_c}{2\epsilon}} \approx 7800 \ \frac{\mathrm{N}}{\mathrm{mm}^2}, \tag{42}$$

see Kuhn [10]. Although the multidimensional case is more complex, this relation provides an estimate of the "virtual" material strength. The wave speed of dilatational waves is

$$c_d = \sqrt{\frac{K + \frac{4}{3}\mu}{\rho}} \approx 7.1 \cdot 10^6 \ \frac{\mathrm{mm}}{\mathrm{s}} \tag{43}$$

and the shear wave speed is

$$c_s = \sqrt{\frac{\mu}{\rho}} \approx 1.6 \cdot 10^6 \ \frac{\mathrm{mm}}{\mathrm{s}} \tag{44}$$

respectively.

Fig. 5 shows the results of the simulation. The contour plots display the hoop stress σ_ϕ. Regions in which the phase field is lower than a threshold of $s < 0.1$ are rendered invisible in order to illustrate the crack. Furthermore, the stress field is plotted on the deformed body, where the deformation is exaggerated by a factor of 30.

The temperature load has reached its final value, i.e. $T(t) = 1.0$, at time $t_e = 10^{-6}$ s. The material starts to expand and a bulge forms at the top and the bottom edge of the specimen. In the interior body however, inertia forces resist this expansion. Consequently, a compressive

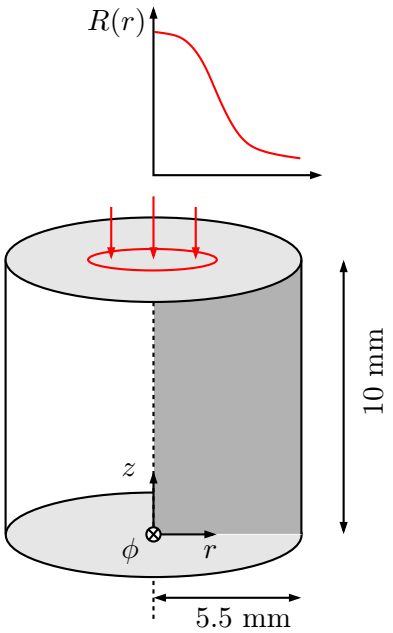

Fig. 2 Cylindrical specimen subjected to a particle beam.

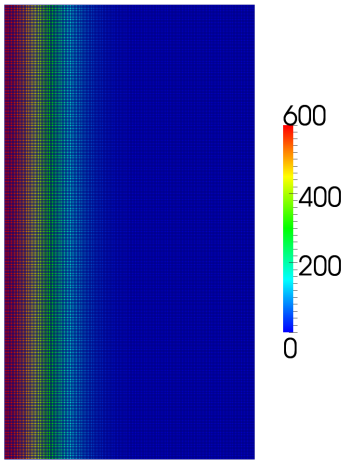

Fig. 3 Finite element mesh and contour plot of the temperature field θ for $g(t) = 1.0$ and $\theta_{\max} = 600°\mathrm{C}$.

Table 1 Material and model parameters

mechanical	phase field	thermal
$E = 1.15 \cdot 10^7 \ \frac{\mathrm{N}}{\mathrm{mm}^2}$	$\epsilon = 0.05$ mm	$\alpha_T = 4 \cdot 10^{-6} \ \frac{1}{K}$
$\nu = 0.3$		$\theta_0 = 0°\mathrm{C}$
$\rho = 1.83 \cdot 10^{-6} \ \frac{\mathrm{kg}}{\mathrm{mm}^3}$		$\theta_{\max} = 600°\mathrm{C}$
$\mathcal{G}_c = 5 \ \frac{\mathrm{N}}{\mathrm{mm}}$		

stress results, see Fig. 5 a). This maximum compressive stress decreases over time as the material further expands. Simultaneously, elastic waves are emitted towards the circumferential surface of the cylinder and the first cracks can be observed, see Fig. 5 c). These cracks nucleate at the upper and lower boundary of the cylinder in regions that experience high shear stress σ_{rz}. This is consistent with the formulation of the elastic energy density (14), that allows for crack propagation under deviatoric or shear load states. At time $t = 8.01 \cdot 10^{-6}$ s further cracks form, see Fig. 5 d). In contrast to the primary shear cracks, the material now breaks in the interior of the body. These cracks grow and branch several times, see Fig. 5 e). The reflection of elastic waves at the boundaries and at the cracks leads to a rather complicated stress field. The final crack pattern is restricted to the region around the axis of the cylinder, which is shattered to pieces, see Fig.5 f). Note that the absolute value of the peak compressive, i.e. negative stress, is much larger than the material strength estimate σ_c but the positive tensile stress does not exceed this limit significantly. This is also a feature of the formulation (14), which models a resistance against crack growth in compression.

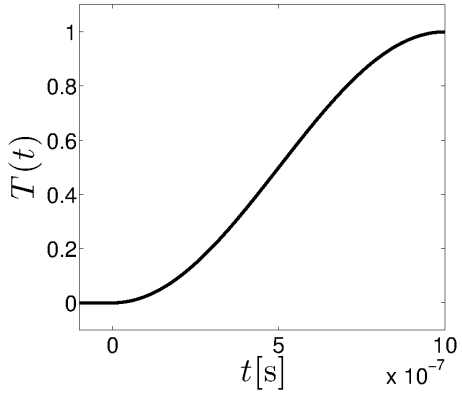

Fig. 4 Function $T(t)$ for $t_e = 10^{-6}$ s.

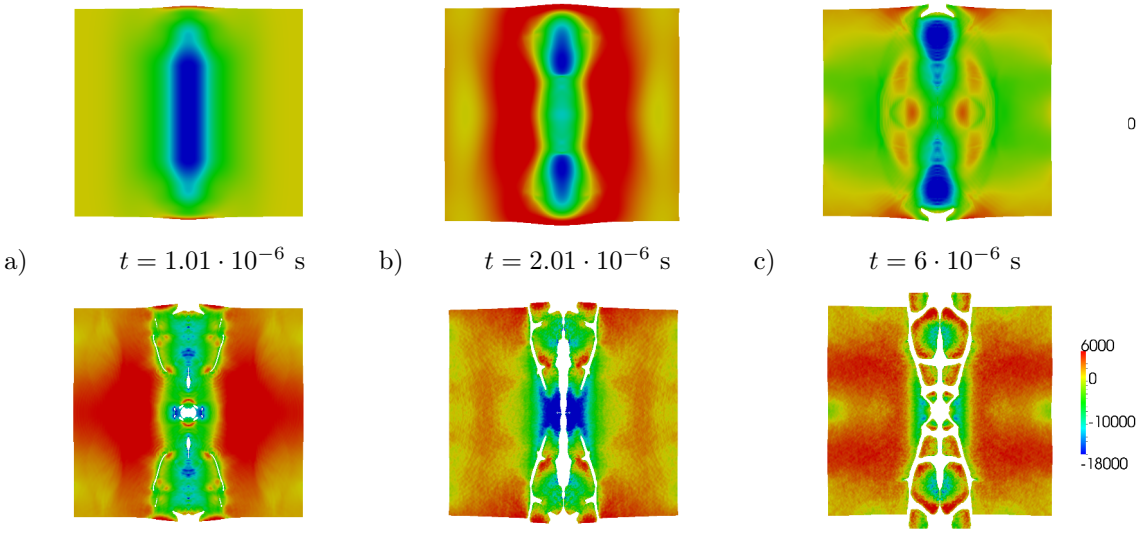

Fig. 5 Hoop stress σ_ϕ in $\left[\frac{\mathrm{N}}{\mathrm{mm}^2}\right]$. Although the finite element model only covers one half of the model, the whole body is restored in a post processing step to enhance the visualization of the results.

Failure of heavy-ion irradiated copper cylinders has been reported in Richter [13]. The cylinders were irradiated by a uranium beam along their axis similar to the situation that is shown in Fig. 2. In the experiments, damage was also confined to the region around the cylinder's axis and the beam cut a 3.8mm deep hole in the target. However, failure was probably not solely due to fracture.

Additional experiments, using thin disc targets subjected to a heavy-ion beam have been conducted by the GSI in fall 2014. Although most specimens failed due to melting or did not fail at all because of the low beam intensity, a copper-diamond specimen showed different signs of damage, see Fig. 6. Here, the beam cut a hole into the specimen and brittle fracture possibly may have played a role in the failure process.

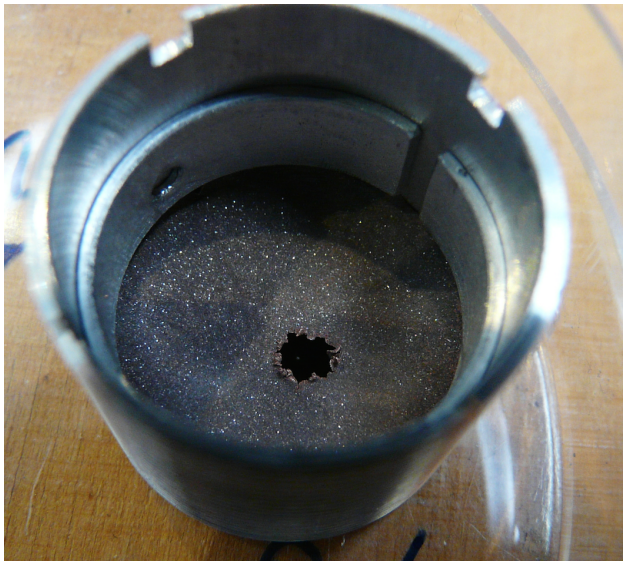

Fig. 6 Beam induced damage in a thin disc made of a copper-diamond composite caused by a short pulse, 125 MeV/u 238U beam with an intensity of 10^{10} ions/pulse. The disc had a thickness of 200 μm and a diameter of 20 mm.

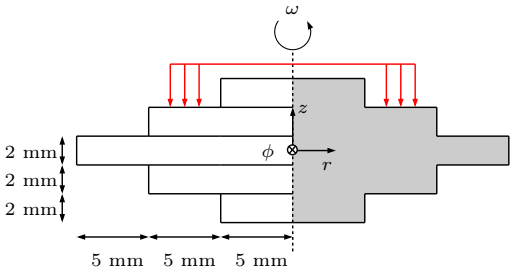

Fig. 7 Disc subjected to a particle beam.

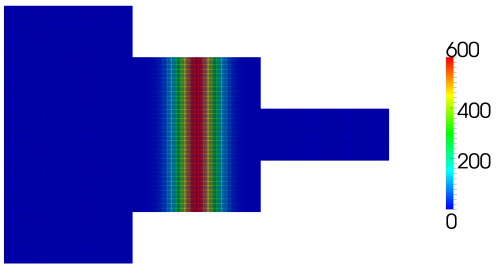

Fig. 8 Finite element mesh and contour plot of the temperature field θ for $g(t) = 1.0$ and $\theta_{\max} = 600°\mathrm{C}$.

4.2 Disc

The second numerical example studies a circular disk, see Fig. 7. The disc is subjected to an annular particle beam as it is shown in Fig. 7. The set up can also be interpreted as a fast rotating disc, where the angular velocity ω advects thermal energy much faster than heat conduction takes place. However, inertia effects due to fast rotation are neglected in the simulations. The loading and the geometry are again axisymmetric, so the model can be reduced to the shaded area. The temperature load is expressed in the form

$$\theta^*(r,t) = \theta_{\max} R(r) T(t). \tag{45}$$

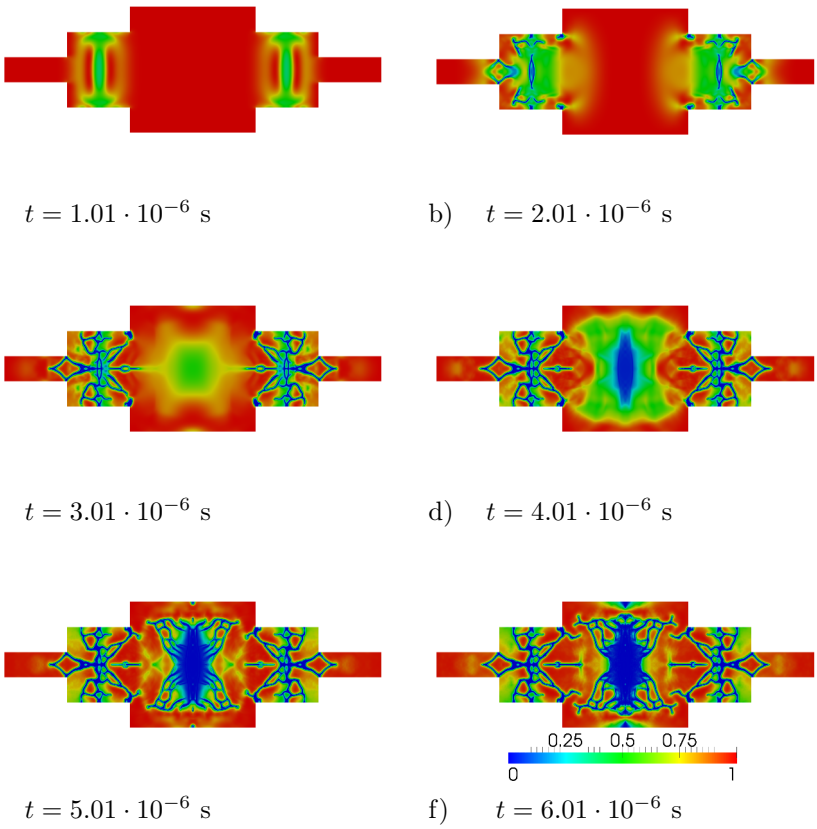

a) $t = 1.01 \cdot 10^{-6}$ s b) $t = 2.01 \cdot 10^{-6}$ s

c) $t = 3.01 \cdot 10^{-6}$ s d) $t = 4.01 \cdot 10^{-6}$ s

e) $t = 5.01 \cdot 10^{-6}$ s f) $t = 6.01 \cdot 10^{-6}$ s

Fig. 9 Contour plots of the phase field s. Although the finite element model only covers one half of the model, the whole body is restored in a post processing step to enhance the visualization of the results.

In this example, the radial distribution $R(r)$ is set to

$$R(r) = \exp\left(-\left(\frac{r - 7.5 \text{ mm}}{r_0}\right)^2\right) \tag{46}$$

where $r_0 = 0.6$ mm. The temperature profile is also shown in Fig. 8 and the function $T(t)$ is the same as in section 4.1. The regular mesh consists of 81000 quadratic elements. Again all boundaries are stress free and the material parameters remain unchanged to the previous example, see table 1.

The results are shown in Fig. 9 as contour plots of the phase field variable s. At first, the phase field drops considerably where the temperature load is applied, see Fig. 9 a). Subsequently, several cracks form in the interior of the body and cracks nucleate at the surfaces of the disc as well. Note the crack nucleation at critical corners which have some kind of a notch effect, see Fig. 9 b). The maximum temperature load is reached at $t_e = 10^{-6}$ s. Dilatational waves start to reach the center of the disc at time $t_c \approx \frac{7.5 \text{ mm}}{c_d} + t_e \approx 2.05 \cdot 10^{-6}$ s. Shortly after that one can once again observe a significant drop of the phase field in a large region, see Fig. 9 c). In contrast to the initial cracks however, final damage, i.e. $s = 0$, is not restricted to thin cracks. Instead, a large region is completely broken material and several thin cracks emerge from this region, see

Fig. 9 d) and Fig. 9 e). Here, it can be assumed that the internal length ϵ is to large to resolve a number of very close thin cracks. Hence, the result is not a set of small cracks but one large region of completely damaged material. The final crack pattern is shown in Fig. 9 f).

5 Summary

This work presents a continuum mechanics approach to dynamic fracture in brittle solids that are subjected to intense high energy particle beams. The model is a so-called phase field model for fracture that represents cracks by means of an additional scalar field variable, the phase field. The core of this model is a variational principle that is based on an energy functional and is closely related to the well-known Griffith's principle of classical fracture mechanics. In addition to the phase field model presented in our previous work [14], thermoelastic effects are included in the present model. Thermoelasticity is modelled by assuming that an increase in temperature leads to volumetric expansion of this material if this is not prohibited by mechanical restraints. In principle, the model also allows to treat heat conduction, although that is not considered in this work. The focus is rather to model pulse like thermal loading where heat conduction is negligible. The approach leads to a set of coupled partial differential equations that are solved numerically. The method we choose is an axisymmetric finite element formulation with implicit time integration. The work concludes with two numerical experiments that illustrate the functionality of our model. Here, the effect of the particle beam is modelled by prescribing a temperature load with a bell-shaped spatial distribution. The examples show that the phase field approach is suited to capture coupled phenomena like thermal fracture.

However, the model could not yet be validated by comparison to experimental results, which is considered to be an important next step. Since the current facility in Darmstadt cannot deliver beams of sufficient intensity to actually cause fracture in most situations, high-power lasers have to be used until FAIR is in service. Furthermore, the temperature-dependence of critical material parameters like the Young's modulus should be taken into account in the future, in order to capture the possibly large changes that occur in material which is hit directly by the beam.

References

1. Amor, H., Marigo, J.J., Maurini, C.: Regularized formulation of the variational brittle fracture with unilateral contact: Numerical experiments. J. Mech. Phys. Solid. **57**(8), 1209–1229 (2009)
2. Boettinger, W.J., Warren, J.A., Beckermann, C., Karma, A.: Phase-field simulation of solidification1. Annual Review of Materials Research **32**(1), 163–194 (2002). DOI 10.1146/annurev.matsci.32.101901.155803
3. Borden, M.J., Verhoosel, C.V., Scott, M.A., Hughes, T.J.R., Landis, C.M.: A phase-field description of dynamic brittle fracture. Comput. Meth. Appl. Mech. Eng. **217–220**, 77–95 (2012)
4. Bourdin, B.: Numerical implementation of the variational formulation of quasi-static brittle fracture. Interfaces Free Bound. **9**, 411–430 (2007)
5. Chambolle, A.: An approximation result for special functions with bounded deformation. J. Math. Pure Appl. **83**(7), 929–954 (2004)
6. Francfort, G.A., Marigo, J.J.: Revisiting brittle fracture as an energy minimization problem. J. Mech. Phys. Solid. **46**(8), 1319–1342 (1998)
7. Griffith, A.A.: The phenomena of rupture and flow in solids. Phil. Trans. Roy. Soc. Lond. A **221**, 163–198 (1921)
8. Hofacker, M., Miehe, C.: A phase field model for ductile to brittle failure mode transition. PAMM **12**(1), 173–174 (2012)
9. Hofacker, M., Miehe, C.: A phase field model of dynamic fracture: Robust field updates for the analysis of complex crack patterns. Int. J. Numer. Meth. Eng. **93**(3), 276–301 (2013)
10. Kuhn, C.: Numerical and analytical investigation of a phase field model for fracture. Phd thesis, Technische Universität Kaiserslautern (2013)
11. Kuhn, C., Müller, R.: Phase field simulation of thermomechanical fracture. PAMM **9**(1), 191–192 (2009)

12. Kuhn, C., Müller, R.: A continuum phase field model for fracture. Eng. Fract. Mech. **77**(18), 3625–3634 (2010). Computational Mechanics in Fracture and Damage: A Special Issue in Honor of Prof. Gross
13. Richter, H., Aiginger, H., Noah Messomo, E.: Simulating transient effects of pulsed beams on beam intercepting devices. Ph.D. thesis, Vienna, Tech. U., Vienna (2011). Presented 14 Oct 2011
14. Schlueter, A., Willenbuecher, A., Kuhn, C., Mueller, R.: Phase field approximation of dynamic brittle fracture. Comput. Mech. pp. 1–21 (2014)
15. Schmitt, R., Kuhn, C., Mueller, R., Bhattacharya, K.: Crystal plasticity and martensitic transformations - a phase field approach. Technische Mechanik **34**(1), 23–38 (2014)
16. Schrade, D., Mueller, R., Xu, B.X., Gross, D.: Domain evolution in ferroelectric materials: A continuum phase field model and finite element implementation. Comput. Meth. Appl. Mech. Eng. **196**(41–44), 4365–4374 (2007)
17. Tahir, N.A., Hoffmann, D.H.H., Maruhn, J.A., Spiller, P., Bock, R.: Heavy-ion-beam-induced hydrodynamic effects in solid targets. Phys. Rev. E **60**, 4715–4724 (1999)